

Microstructure at morphotropic phase boundary in $\text{Pb}(\text{Mg}_{1/3}\text{Nb}_{2/3})\text{O}_3\text{-PbTiO}_3$ ceramic: Coexistence of nano-scaled {110}-type rhombohedral twin and {110}-type tetragonal twin

Haijun Wu, Dezheng Xue, Duchao Lv, Jinghui Gao, Shengwu Guo et al.

Citation: *J. Appl. Phys.* **112**, 052004 (2012); doi: 10.1063/1.4745935

View online: <http://dx.doi.org/10.1063/1.4745935>

View Table of Contents: <http://jap.aip.org/resource/1/JAPIAU/v112/i5>

Published by the [American Institute of Physics](#).

Related Articles

Influence of grain boundary properties on spall strength: Grain boundary energy and excess volume
J. Appl. Phys. **112**, 083529 (2012)

Naturally asymmetrical double-Schottky barrier model: Based on observation of bicrystal
Appl. Phys. Lett. **101**, 173508 (2012)

Direct measurement of grain boundary enthalpy of cubic yttria-stabilized zirconia by differential scanning calorimetry
J. Appl. Phys. **112**, 083527 (2012)

Depressed scattering across grain boundaries in single crystal graphene
Appl. Phys. Lett. **101**, 172107 (2012)

Effect of interfacial lattice mismatch on bulk carrier concentration and band gap of InN
J. Appl. Phys. **112**, 083521 (2012)

Additional information on *J. Appl. Phys.*

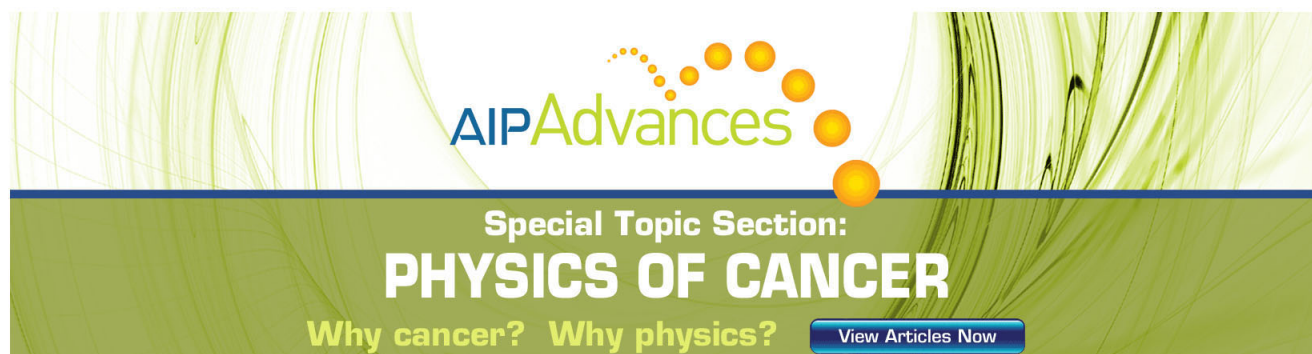
Journal Homepage: <http://jap.aip.org/>

Journal Information: http://jap.aip.org/about/about_the_journal

Top downloads: http://jap.aip.org/features/most_downloaded

Information for Authors: <http://jap.aip.org/authors>

ADVERTISEMENT



AIPAdvances

Special Topic Section:
PHYSICS OF CANCER

Why cancer? Why physics? [View Articles Now](#)

Microstructure at morphotropic phase boundary in $\text{Pb}(\text{Mg}_{1/3}\text{Nb}_{2/3})\text{O}_3\text{-PbTiO}_3$ ceramic: Coexistence of nano-scaled $\{110\}$ -type rhombohedral twin and $\{110\}$ -type tetragonal twin

Haijun Wu,^{1,a)} Dezheng Xue,^{1,2,b)} Duchao Lv,¹ Jinghui Gao,^{1,2} Shengwu Guo,¹ Yumei Zhou,¹ Xiangdong Ding,¹ Chao Zhou,¹ Sen Yang,¹ Yaodong Yang,¹ and Xiaobing Ren^{1,2}

¹Multi-disciplinary Materials Research Center, Frontier Institute of Science and Technology,

State Key Laboratory for Mechanical Behavior of Materials, Xi'an Jiaotong University, Xi'an 710049, China

²Ferroic Physics Group, National Institute for Materials Science, Tsukuba, 305-0047 Ibaraki, Japan

(Received 20 October 2011; accepted 27 March 2012; published online 4 September 2012)

For more than half a century, the morphotropic phase boundary (MPB) has drawn constant interest in developing piezoelectric materials, as the phase instability at the region significantly enhances piezoelectricity. However, the local structure/symmetry at the MPB region is still under controversy. The investigation on morphology and origin of the local structure at MPB is of considerable importance to provide a microstructure basis for high piezoelectricity. In the present study, we thus use high resolution transmission electron microscopy to investigate the microstructure feature of MPB at PMN-PT ceramics. The local structure is shown to be the coexistence of nano-scaled $\{110\}$ -type rhombohedral (R) twin and $\{110\}$ -type tetragonal (T) twin. Such nano-scaled coexistence can be due to a nearly vanishing polarization anisotropy and low domain wall energy at MPB, which thus facilitates polarization rotation between $\langle 001 \rangle_T$ and $\langle 111 \rangle_R$ states and leads to high properties of MPB compositions. © 2012 American Institute of Physics. [<http://dx.doi.org/10.1063/1.4745935>]

I. INTRODUCTION

Piezoelectric materials, acting as converters between mechanical and electrical energies, have found various applications in many fields such as medical imaging, non-invasive treatment, micro-speaker, gas lighter, and so on.^{1,2} In general, the common approach to achieve high piezoelectricity is to place the materials at the morphotropic phase boundary (MPB) between two ferroelectric phases in their phase diagrams.^{2–5} Following such a guideline, many piezoelectric families, such as the $\text{PbZrO}_3\text{-PbTiO}_3$ (PZT) ceramic, the $\text{Pb}(\text{Mg}_{1/3}\text{Nb}_{2/3})\text{O}_3\text{-PbTiO}_3$ (PMN-PT), and $\text{Pb}(\text{Zn}_{1/3}\text{Nb}_{2/3})\text{O}_3\text{-PbTiO}_3$ (PZN-PT) single crystal, have been developed to possess high piezoelectricity and been widely used in industry and daily life.

Although the high piezoelectricity can be achieved at MPB region, there are still questions that have not been completely understood, especially those related with the microstructure. The microstructure, like the ferroelectric domains, largely controls the piezoelectric performance, thus intensive studies have been focused on the domain morphology and the corresponding crystallographic features of MPB.^{6,7} Nevertheless, the exact local structure at MPB region is still under controversy with several assumptions like the single phase assumption,^{8–11} the adaptive phase assumption,^{12–17} and the coexistence assumption.^{18–27}

The existence of single phase, monoclinic (M) (Refs. 8–10) or orthorhombic (O),¹¹ in the MPB region was proposed, based on the high resolution x-ray powder diffraction (XRD)

profile. However, recent studies have shown that the domain morphology at MPB is nanodomains.^{28–31} The key evidence of single phase assumption, i.e., the appearance of intensity in diffraction patterns that formerly linked to a single phase, can be a result of coherence effects among nanodomains as well, even without knowing the local structure within each nanodomain.^{8–10,12–17,28–30,32–34} Furthermore, M or O phase is not stable based on Landau theory, compared with the rhombohedral (R) and tetragonal (T) phase, especially when temperature approaches to the Curie temperature.³⁵

Considering the problems of the single phase assumption, Viehland^{12,13} and Wang^{15–17} proposed a model to point out that the reported M or O is just an adaptive state with only nano-twinning R or only nano-twinning T . Recently, Zhu *et al.*^{32–34} investigated the hierarchical domain morphology in PMN-PT single crystal near the MPB region by analytical electron microscopy to support this theoretical assumption. However, the experimental results seem to vary between O phase and M phase with the orientation and composition,^{32–34} thus a convincing conclusion cannot be made. Since the MPB region can be regarded as a bridge between the ferroelectric R and T phases, intuitively only one single nano-twinning phase (either T nano-twin^{32,33} or R nano-twin³⁴) exists at MPB is incomplete.

Cao and Cross¹⁸ proposed a statistical model to address that the T and R phase coexist around MPB. The presence of coexisted structural modifications (R and T) would enhance the instability of the material to an applied external electric field due to a possible combination of six polarization directions ($\langle 001 \rangle_T$) in the T phase and eight ($\langle 111 \rangle_R$) in the R phase.¹⁹ Recent calculations by Rossetti have shown the R and T coexistence, especially in nanoscale, can be stable.^{24–27} Based on their calculations, the MPB possesses an adaptive phase with

^{a)}Electronic mail: wuhaijunnavy@gmail.com.

^{b)}Electronic mail: xuedezhen@gmail.com.

coexisted *R* and *T* nanodomains, rather than only nano-scaled *R* or *T* as the adaptive phase assumption proposed.^{24–27} Some high resolution XRD profiles and their reciprocal space mapping results with average structural information have shown that the MPB region is coexisted *R* nanotwin and *T* nanotwin.^{36–39} However, up to now, no direct and convincing evidences to nano-scaled *R* and *T* coexistence around MPB have been provided.

In the present work, we thus study the microstructure at the MPB region by high resolution transmission electron microscopy (HREM) using PMN-PT ceramics. Combining the advantage of high spatial resolution of HREM and the twin diffraction pattern (TDP) analysis of *R* twin and *T* twin,⁴⁰ we tried to identify the local structure of MPB. Finally, the vanishing anisotropy of polarization rotation and nearly-zero domain wall energy at MPB are suggested to result in the nano-scaled local structure.

II. EXPERIMENTAL PROCEDURES

PMN-*x*PT ceramics with $20 \leq x \leq 40$ were synthesized by a modified “columbite-type” route⁴¹ using the powders of PbO (>99%), MgO (>99.5%), Nb₂O₅ (>99.95%), and TiO₂ (>99.9%). The pure precursor powder of MgNb₂O₆ was mixed with TiO₂ and MgO. An excess of PbO of 2 mol. % was added to the mixed powders in order to compensate the lead loss during calcination and sintering. Samples were calcined at 900 °C for 4 h. Then pellets were cold pressed and sintered at 1250 °C for 3 h covered with the same composition powder as a lead protection in sealed crucibles. The sintered samples for dielectric measurement were polished to obtain the parallel sides, ultrasonically cleaned, and then painted with silver electrodes. The dielectric permittivity was measured at 100 kHz using a HP HIOKI LCR meter. Average structural information was collected by an *in-situ* XRD measurement with the temperature accuracy about ± 5 °C. The samples for XRD measurement were annealed at

250 °C for 8 h to release the possible internal stress by polishing.

Sample preparation for TEM investigations was done by subsequent cutting, polishing, dimpling, and ion milling. The TEM experiments were carried out on a JEM-2100F microscope at an accelerating voltage of 200 kV. HREM images are recorded with fast-scan CCD. Image filtering and processing were conducted using Digitalmicrograph software (Gatan, USA).

III. RESULTS

A. In-situ XRD and dielectric permittivity

The permittivity vs. temperature curve, as shown in Fig. 1(a), reveals a broad dielectric anomaly between -10 °C and 75 °C with fairly large thermal hysteresis. Such anomaly indicates a sluggish phase transition over a wide temperature range, conventionally being linked to MPB phenomenon. *In-situ* XRD results upon heating were shown in Figs. 1(b)–1(d). The diffraction profiles at -100 °C and 94 °C correspond to *R* symmetry and *T* symmetry, respectively. At MPB state of 12 °C and 52 °C, being around the permittivity anomaly, the peak profiles are consistent with a superposition of *T* and *R* profiles. This could suggest that MPB is composed of coexisted *R* and *T* phases. Furthermore, in MPB region, with increasing temperature, the intensity of *T* profile increases gradually. Due to such sluggish nature of the transformation between *R* and *T*, the MPB state appears in a wide temperature range.

It is noted that one common feature in the high performance systems, like PZT,¹ PMN-PT,^{10,42} PZN-PT,⁴³ Ba(Zr_{0.2}Ti_{0.8})O_{3-x}(Ba_{0.7}Ca_{0.3})TiO₃ (BZT-BCT),^{3,44–46} and Ba(Sn_{0.12}Ti_{0.18})O_{3-x}(Ba_{0.7}Ca_{0.3})TiO₃ (BST-BCT),⁴⁷ is the existence of a C-R-T triple point in their phase diagram. For the Pb-free systems, BZT-BCT and BTS-BCT, such triple point is proved to be a tricritical point (TCP) by the vanishing

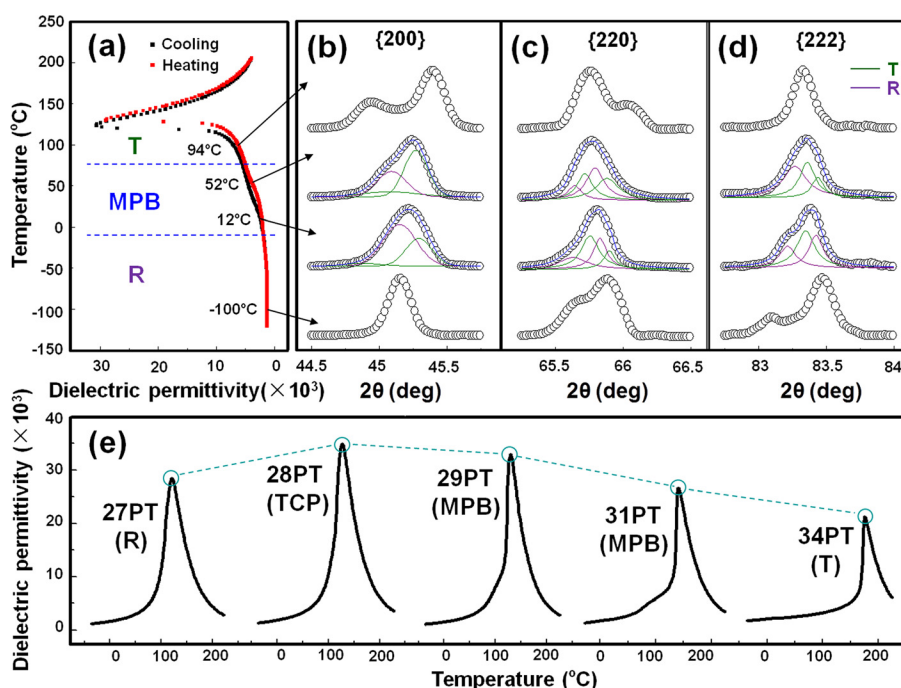


FIG. 1. (a) Permittivity vs. temperature curve of PMN-32PT; (b)–(d) *In-situ* x-ray diffraction profiles of the PMN-32PT during heating; (e) the temperature dependence of dielectric permittivity for PMN-*x*PT ($x = 27, 28, 29, 31, 34$).

thermal hysteresis and highest transition permittivity peak at the point. For the similarity of phase diagram between these Pb-free systems and PMN-PT, the triple point in PMN-PT system is likely to be a TCP. Fig. 1(e) shows the dielectric permittivity vs. temperature for different compositions. The transition permittivity peak is highest at the triple-point composition, PMN-28PT, and decreases with deviating from the triple point. This suggests that PMN-PT system possesses a TCP, but further experimental conformation is still needed.

B. Domain morphology at the MPB

The domain morphology evolution from *R* composition through MPB to *T* composition is shown in Fig. 2. At *R* side (PMN-28PT), herringbone-like domain configuration is shown in Fig. 2(a), in which broad and narrow domains are not strictly alternating. At *T* side (PMN-34PT), bimodal and lamellar domain distribution is shown in Fig. 2(b), which is recognized by a lamellar structure of 90° domains with strict alternation between narrow and broad microdomains.

Three types of nanodomains can be found at MPB in PMN-32PT, as shown in Figs. 2(c1)–2(c3). The hierarchical domain pattern^{32–34} is shown in Fig. 2(c1), where two traces of nanodomains interact with each other and form lamellar submicrodomains. Such domain pattern is more obvious in PMN-PT single crystal.^{32–34} But in PMN-PT ceramic, another type of nanodomain is more widespread, i.e., two traces of nanodomains without lamellar submicrodomains distribute in different areas (shown in Fig. 2(c2)). The third type nanodomain is only along one direction, as shown in Fig. 2(c3). With composition change, the domain structure changes from an *R* herringbone structure (Fig. 2(a)) through MPB nano-scaled domains (Figs. 2(c1)–2(c3)) to a lamellar *T* configuration (Fig. 2(b)).

C. Local structure of MPB by HREM

Recently, nano-twinning structure around MPB has been extensively reported in theory and experiment.^{13,14,17,32–34,36,39} If there is a coexistence of nano-scaled *R* twin and *T* twin

at MPB region, the corresponding diffraction pattern would reflect as a superposition effect of both *R* twin and *T* twin. For PMN-PT, the lattice difference between *R* and *T* is too small to differentiate in select area electron diffraction (SAED) pattern, especially for the nano-scaled domains. We, thus, choose Fast Fourier transform (FFT) of HREM image to differentiate the *R* nano-twins and *T* nano-twins.

Fig. 3 shows HREM and its FFT evidence for the coexistence of nano-scaled *R* twin and *T* twin on [010] zone axis. Figs. 3(a1) and 3(a2) show the simulated twin diffraction pattern for (110)-type *R* twin and (011)-type *T* twin on [010] zone axis. In the TDP, there are two key features that can reflect the structure information of the twin:^{48–55} the unsplit row of reflection spots (USR)^{48,49,51,56,57} and the spot splitting.^{48–51,56} The unsplit row of reflection spots, contributed by two twin variants with coincident lattices in reciprocal space, corresponds to the twin plane which shared between two twin variants in real space (USR ⊥ twin plane).^{48,49,51,56,57} Spot splitting (Δg , the discrepancy of *g* vectors) is caused by a slight discrepancy in simultaneously reflecting *g* vectors from two individual crystal variants; In other words, $\Delta g = g_1 - g_2$ is due to the obliquity of the twins.^{48–53,56} The widely accepted TDP phenomenon, $\Delta g // \text{USR}$, can only be observed along certain zone axis (zone axis ⊥ twin plane), however on other zone axes, the relation is different.^{51,56,57} The details will appear elsewhere.⁴⁰ The (110)-type *R* twin with polarization direction along [111]/[11-1] and (011)-type *T* twin with polarization direction along [010]/[001] have the same Δg along [001], but different USR. Thus, the overlying TDP of *R* with *T* is expected to have all the reflection spots splitting along [001] without USR. Fig. 3(b) is a HREM image including several nanodomains of MPB. Its FFT image in Fig. 3(c) shows that all the reflection spots are splitting (or elongating) along [001]. For the 100 reflection spots, they split along [001] in *R*-twin diffraction pattern (Fig. 3(a1)) but are on the USR in *T*-twin diffraction pattern (Fig. 3(a2)). The experimentally observed

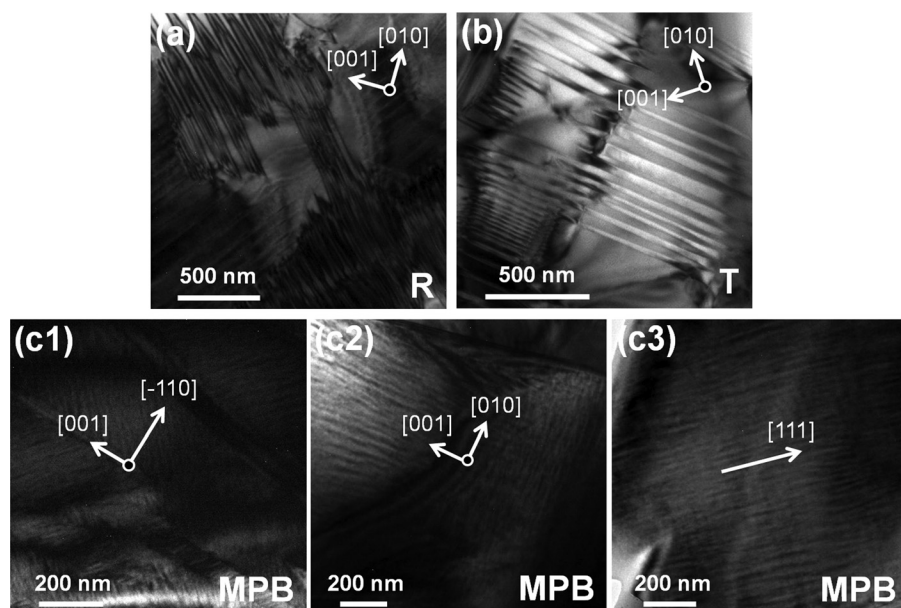


FIG. 2. Bright field (BF) micrographs of PMN-xPT ceramic. (a) BF image of PMN-28PT shows lamellar herringbone like domain configuration of ferroelectric *R* phase; (b) BF image of PMN-34PT shows bimodal domain distribution of ferroelectric *T* phase. (c1)–(c3) BF images of PMN-32PT show three types of nano-domain patterns for MPB: (c1) hierarchical domain pattern; (c2) two traces of nanodomains without lamellar submicrodomains; (c3) only one trace of nanodomains.

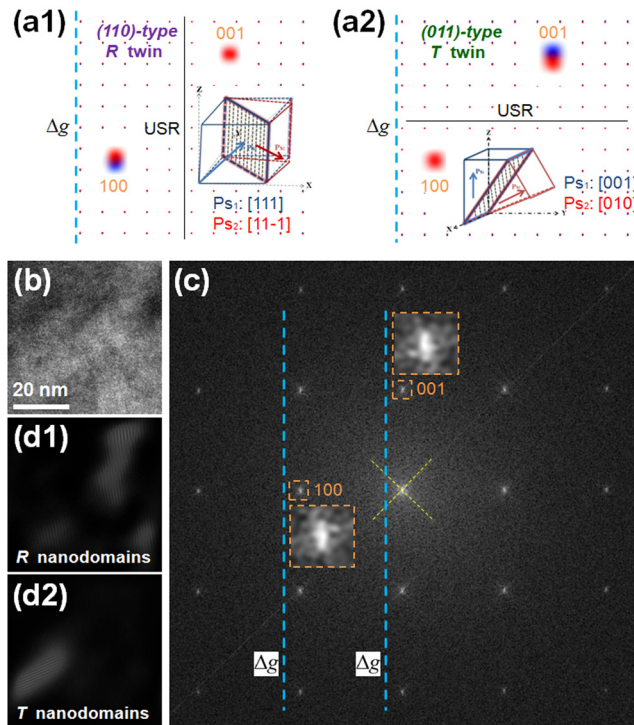


FIG. 3. HREM and its FFT evidence for the coexistence of nano-scaled *R* twin and *T* twin. (a1) and (a2) show the simulated twin diffraction pattern for *R* twin and *T* twin on [010] zone axis, respectively. In order to see the unsplit row of reflections (USR) and spot splitting (Δg) clearly, the enlarged 001 and 100 reflections are shown aside. The schematic figure is the related twin structure: (110)-type *R* twin with polarization direction along [111] and [11-1], while (011)-type *T* twin with polarization direction along [001] and [010]. Overlying (a1) and (a2) can reflect as a superimposing effect between *R* twin and *T* twin; (b) HREM image of MPB nanodomains with the electron beam incident along the [010] direction; (c) Fast Fourier transform of image (b) shows all the reflection spots splitting or elongating along [001], and the splitting/elongating on 100 and 001 reflection spots is from *R* nanodomains and *T* nanodomains, respectively. The image was tilted to a certain angle, and the original direction was shown as yellow dashed lines; (d1) A Fourier-filtered image, where only 100 reflection spots are included, shows the distribution of *R* nanodomains; (d2) A Fourier-filtered image, where only 001 reflection spots are included, shows the distribution of *T* nanodomains.

splitting/elongating of 100 reflection spots is thus caused by *R* nanodomains. Therefore, the image of inverse Fourier-filtered transform (IFFT) of 100 reflection spots can show the distribution of *R* nanodomains as shown in Fig. 3(d1). Similarly, the splitting/elongating of 001 reflection spots are caused by *T* nanodomains, as the 001 reflection spots are on the USR in *R*-twin diffraction pattern (Fig. 3(a1)), but split along [001] in *T*-twin diffraction pattern (Fig. 3(a2)). Therefore, the IFFT image of 001 reflection spots in Fig. 3(d2) can reflect the distribution of *T* nanodomains.

Fig. 4 shows HREM and its FFT evidence for the coexistence of nano-scaled *R* twin and *T* twin on [110] zone axis. The simulated TDPs for (110)-type *R* twin and (110)-type *T* twin along [110] zone axis are shown in Figs. 4(a1) and 4(a2). The (110)-type *R* twin and (110)-type *T* twin have the same Δg along [-112], but different USR. Fig. 4(b) is a HREM image including several nanodomains of MPB. Its FFT image in Fig. 4(c) shows that all the reflection spots are splitting (or elongating) along [-112] without USR, which

can agree with the overlapping result of Figs. 4(a1) and 4(a2). The -111 reflection spots split along [-112] in *R*-twin diffraction pattern (Fig. 4(a1)), while are on the USR in *T*-twin diffraction pattern (Fig. 4(a2)), and the experimentally observed splitting/elongating of -111 reflection spots in Fig. 4(c) is caused by *R* nanodomains. Thus, IFFT image of -111 (Fig. 4(d1)) reflection spots can show the distribution of *R* nanodomains. On the contrast, the splitting/elongating of 002 reflection spots are caused by *T* nanodomains, as the 002 reflection spots are on the USR in *R*-twin diffraction pattern (Fig. 4(a1)), while split along [-112] in *T*-twin diffraction pattern (Fig. 4(a2)). Thus, the IFFT image of 0-20 reflection spots can reflect the distribution of *T* nanodomains as shown in Fig. 4(d2).

It should be noted that the slim nanodomains along a certain direction in HREM image (real space) would reflect as spot elongating³⁴ along another direction in FFT (reciprocal space), which are perpendicular to each other. Such spot elongating caused by slim nanodomains often overlaps the spot splitting caused by *g*-vectors discrepancy from two individual crystal variants. Fortunately, the spot elongating direction is parallel to the spot splitting direction in the twin diffraction pattern. Thus, the spot elongating phenomenon in FFT pattern can be used to distinguish the nano-scaled *R* twin and *T* twin.

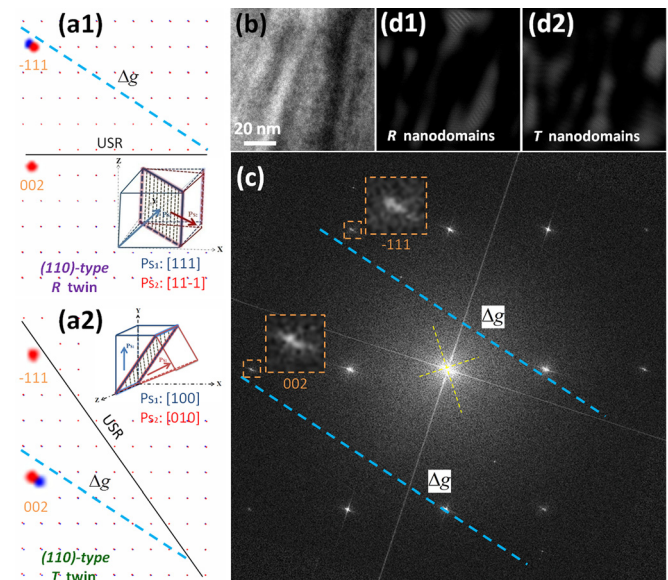


FIG. 4. HREM and its FFT evidence for the coexistence of nano-scaled *R* twin and *T* twin. (a1) and (a2) show the simulated twin diffraction pattern for *R* twin and *T* twin on [110] zone axis, respectively. In order to see the USR and Δg clearly, the enlarged 002 and -111 reflections are shown aside. The schematic figure is the related twin structure: (110)-type *R* twin with polarization direction along [111] and [11-1], while (110)-type *T* twin with polarization direction along [100] and [010]. Overlying (a1) and (a2) can reflect as a superimposing effect between *R* twin and *T* twin; (b) HREM image of MPB nanodomains with the electron beam incident along the [110] direction; (c) Fast Fourier transform of image (b) shows all the reflection spots splitting or elongating along [-112] and the splitting/elongating on -111 and 002 reflection spots is from *R* nanodomains and *T* nanodomains, respectively. The image was tilted to a certain angle, and the original direction was shown as yellow dashed lines; (d1) An IFFT image, where only -111 reflection spots are included, shows the distribution of *R* nanodomains; (d2) An IFFT image, where only 002 reflection spots are included, shows the distribution of *T* nanodomains.

IV. DISCUSSION

It has been shown in Fig. 2 that the domain size is reduced to nanometer dimensions for compositions located around MPB, comparing with the lamellar like domains of the R and T phase region. The sharp reduction of the conventional micro-scaled domain structure to nano-scaled one is actually a reflection of a drastic decrease in the domain wall energy. As evidenced by transition permittivity peak anomaly in Fig. 1(e), the triple point in the PMN-PT system is likely to be a tricritical point. Its continuous nature would make the MPB compositions possess a weak polarization anisotropy, which yields a low energy barrier between $\langle 001 \rangle_T$ and $\langle 111 \rangle_R$ polarization states and enables an easy polarization rotation. Therefore, the domain wall energy, determined by the energy cost of polarization change within the domain boundary layer,^{26,58} will drastically decrease. Consequently, the nano-scaled domains will appear and the high dielectric and piezoelectric properties can be obtained at MPB.

Strictly speaking, it should be noted that high piezoelectricity not only requires a low anisotropy but also a softening of the lattice.^{3,59} Fortunately, the coexisted R nano-twins and T nano-twins, just as shown in Figs. 3 and 4, can alleviate the transformation stress between the R state and T state, which makes the lattice soft.^{36–39} Thus, such local structure of MPB can get a low polarization anisotropy and elastic softening hand in hand, both contributing to a high piezoelectricity.

Since the nanodomain size is much smaller than the coherent length of diffraction radiation, scattered waves from individual nanodomain coherently will superimpose during diffraction, and thus, significant broadening of reflection spots is expected. The existence of the coexisted nanodomains or nanotwins can be easily taken as M phases or O due to the averaging effect in both polarizing microscopy and x-ray diffraction.

V. SUMMARY

In the present study, we found that the local structure of MPB at PMN-PT ceramics is the coexistence of nano-scaled $\{110\}$ -type R twin and $\{110\}$ -type T twin. We suggest that such nano-scaled coexistence can be due to a nearly vanishing polarization anisotropy and low domain wall energy at MPB. The coexistence could facilitate polarization rotation between $\langle 001 \rangle_T$ and $\langle 111 \rangle_R$ states and leads to high dielectric and piezoelectric properties at MPB compositions.

ACKNOWLEDGMENTS

The authors acknowledge the support of National Basic Research Program of China (2012CB619401 and 2010CB631003), National Natural Science Foundation of China (50720145101, 50771079, 51072158, and 51071117), as well as 111 project of China (B06025).

¹B. Jaffe, W. R. Cook, and H. L. Jaffe, *Piezoelectric Ceramics* (Academic, London, 1971), Vol. 3.

²K. Uchino, *Ferroelectric Devices* (CRC, 2000), Vol. 16.

³W. F. Liu and X. B. Ren, *Phys. Rev. Lett.* **103**, 257602 (2009).

⁴D. Damjanovic, *J. Am. Ceram. Soc.* **88**, 2663 (2005).

⁵Y. U. Wang, *J. Mater. Sci.* **44**, 5225 (2009).

⁶N. Balke, I. Bdikin, S. V. Kalinin, and A. L. Kholkin, *J. Am. Ceram. Soc.* **92**, 1629 (2009).

⁷S. V. Kalinin, B. J. Rodriguez, A. Y. Borisevich, A. P. Baddorf, N. Balke, H. J. Chang, L. Q. Chen, S. Choudhury, S. Jesse, and P. Maksymovych, *Adv. Mater.* **22**, 314 (2010).

⁸B. Noheda, D. E. Cox, G. Shirane, S. E. Park, L. E. Cross, and Z. Zhong, *Phys. Rev. Lett.* **86**, 3891 (2001).

⁹B. Noheda, R. Guo, L. E. Cross, S. E. Park, D. E. Cox, and G. Shirane, *Phys. Rev. Lett.* **84**, 5423 (2000).

¹⁰Z. G. Ye, B. Noheda, M. Dong, D. Cox, and G. Shirane, *Phys. Rev. B* **64**, 184114 (2001).

¹¹Y. P. Guo, H. S. Luo, K. P. Chen, H. Q. Xu, X. W. Zhang, and Z. W. Yin, *J. Appl. Phys.* **92**, 6134 (2002).

¹²Y. M. Jin, Y. U. Wang, A. G. Khachatryan, J. F. Li, and D. Viehland, *J. Appl. Phys.* **94**, 3629 (2003).

¹³Y. M. Jin, Y. U. Wang, A. G. Khachatryan, J. F. Li, and D. Viehland, *Phys. Rev. Lett.* **91**, 197601 (2003).

¹⁴D. Viehland, *J. Appl. Phys.* **88**, 4794 (2000).

¹⁵Y. U. Wang, *Phys. Rev. B* **74**, 104109 (2006).

¹⁶Y. U. Wang, *Phys. Rev. B* **73**, 014113 (2006).

¹⁷Y. U. Wang, *Phys. Rev. B* **76**, 024108 (2007).

¹⁸W. W. Cao and L. E. Cross, *Phys. Rev. B* **47**, 4825 (1993).

¹⁹M. J. Hoffmann, M. Hammer, A. Endriss, and D. C. Lupascu, *Acta Mater.* **49**, 1301 (2001).

²⁰D. Damjanovic, *Appl. Phys. Lett.* **97**, 062906 (2010).

²¹M. Haun, E. Furman, S. Jang, and L. Cross, *Ferroelectrics* **99**, 13 (1989).

²²Y. Ishibashi and M. Iwata, *Jpn. J. Appl. Phys., Part 1* **37**, 985 (1998).

²³A. Khachatryan, *Philos. Mag.* **90**, 37 (2010).

²⁴G. A. Rossetti and A. A. Heitmann, *Philos. Mag.* **90**, 71 (2010).

²⁵G. A. Rossetti and A. G. Khachatryan, *Appl. Phys. Lett.* **91**, 072909 (2007).

²⁶G. A. Rossetti, A. G. Khachatryan, G. Akcay, and Y. Ni, *J. Appl. Phys.* **103**, 114113 (2008).

²⁷G. A. Rossetti, W. Zhang, and A. G. Khachatryan, *Appl. Phys. Lett.* **88**, 072912 (2006).

²⁸L. A. Schmitt, K. A. Schonau, R. Theissmann, H. Fuess, H. Kungl, and M. J. Hoffmann, *J. Appl. Phys.* **101**, 074107 (2007).

²⁹K. A. Schonau, L. A. Schmitt, M. Knapp, H. Fuess, R. A. Eichel, H. Kungl, and M. J. Hoffmann, *Phys. Rev. B* **75**, 184117 (2007).

³⁰R. Theissmann, L. A. Schmitt, J. Kling, R. Schierholz, K. A. Schonau, H. Fuess, M. Knapp, H. Kungl, and M. J. Hoffmann, *J. Appl. Phys.* **102**, 024111 (2007).

³¹A. Kholkin, I. Bdikin, D. Kiselev, V. Shvartsman, and S. H. Kim, *J. Electroceram.* **19**, 83 (2007).

³²J. Zhu, H. Wang, N. Lu, A. A. Bokov, Z. G. Ye, and X. W. Zhang, *Appl. Phys. Lett.* **89**, 042908 (2006).

³³J. Zhu, H. Wang, X. W. Zhang, Y. X. Tang, and H. S. Luo, *Appl. Phys. Lett.* **92**, 132906 (2008).

³⁴J. Zhu, H. Wang, X. W. Zhang, Y. X. Tang, and H. S. Luo, *J. Am. Ceram. Soc.* **91**, 2382 (2008).

³⁵D. Vanderbilt and M. H. Cohen, *Phys. Rev. B* **63**, 094108 (2001).

³⁶W. S. Chang, L. C. Lim, P. Yang, and C. S. Tu, *Appl. Phys. Lett.* **93**, 082903 (2008).

³⁷L. C. Lim, W. S. Chang, K. K. Rajan, M. Shanthi, P. Yang, H. O. Moser, C. S. Tu, F. T. Wang, C. T. Tseng, A. S. Bhalla, and R. Guo, *J. Appl. Phys.* **103**, 084122 (2008).

³⁸L. C. Lim, W. S. Chang, P. Yang, C. S. Tu, F. T. Wang, and C. T. Tseng, *J. Appl. Phys.* **104**, 054102 (2008).

³⁹C. S. Tu, C. M. Hsieh, R. R. Chien, V. H. Schmidt, F. T. Wang, and W. S. Chang, *J. Appl. Phys.* **103**, 074117 (2008).

⁴⁰H. Wu and X. Ren (unpublished).

⁴¹S. L. Swartz and T. R. Shrout, *Mater. Res. Bull.* **17**, 1245 (1982).

⁴²B. Noheda, D. E. Cox, G. Shirane, J. Gao, and Z. G. Ye, *Phys. Rev. B* **66**, 054104 (2002).

⁴³J. Forrester, R. Piltz, E. Kisi, and G. McIntyre, *J. Phys.: Condens. Matter* **13**, L825 (2001).

⁴⁴H. X. Bao, C. Zhou, D. Z. Xue, J. H. Gao, and X. B. Ren, *J. Phys. D: Appl. Phys.* **43**, 465401 (2010).

⁴⁵J. Gao, D. Xue, Y. Wang, D. Wang, L. Zhang, H. Wu, S. Guo, H. Bao, C. Zhou, and W. Liu, *Appl. Phys. Lett.* **99**, 092901 (2011).

⁴⁶D. Z. Xue, Y. M. Zhou, H. X. Bao, C. Zhou, J. H. Gao, and X. B. Ren, *J. Appl. Phys.* **109**, 054110 (2011).

- ⁴⁷X. Dezhen, Z. Yumei, B. Huixin, G. Jinghui, Z. Chao, and R. Xiaobing, *Appl. Phys. Lett.* **99**, 122901 (2011).
- ⁴⁸S. Y. Cheng, N. J. Ho, and H. Y. Lu, *J. Am. Ceram. Soc.* **91**, 1244 (2008).
- ⁴⁹H. Y. Lu, S. Y. Cheng, and N. J. Ho, *J. Am. Ceram. Soc.* **89**, 2177 (2006).
- ⁵⁰E. Polychroniadis and J. Stoemenos, *J. Mater. Sci.* **17**, 2077 (1982).
- ⁵¹W. L. Wang and H. Y. Lu, *J. Am. Ceram. Soc.* **89**, 281 (2006).
- ⁵²F. M. Morales and M. Ruhle, *Acta Crystallogr. B* **62**, 761 (2006).
- ⁵³Y. Yoshimura, A. Kojima, N. Tokunaga, K. Tozaki, and T. Koganezawa, *Phys. Lett. A* **353**, 250 (2006).
- ⁵⁴P. A. Thomas and D. S. Keeble, *J. Appl. Crystallogr.* **42**, 480 (2009).
- ⁵⁵Y. Yoshimura, M. Morioka, A. Kojima, N. Tokunaga, T. Koganezawa, and K. Tozaki, *Phys. Lett. A* **367**, 394 (2007).
- ⁵⁶H. Y. Lu, S. Y. Cheng, and N. J. Ho, *J. Am. Ceram. Soc.* **91**, 2298 (2008).
- ⁵⁷C. Boulesteix, J. Van Landuyt, and S. Amelinckx, *Phys. Status Solidi A* **33**, 595 (1976).
- ⁵⁸M. E. Lines and A. M. Glass, *Principles and Applications of Ferroelectrics and Related Materials* (Oxford University Press, USA, 2001).
- ⁵⁹M. Iwata, H. Orihara, and Y. Ishibashi, *Ferroelectrics* **266**, 57 (2002).